Analytical Methods

Accepted Manuscript

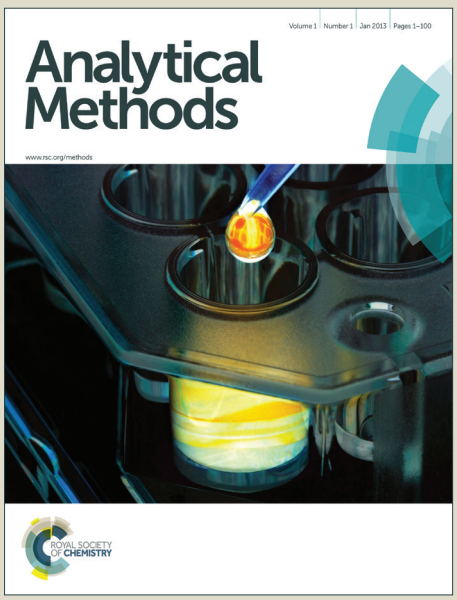

ROYAL SOCIETY OF CHEMISTRY

www.rsc.org/methods

Journal Name

ARTICLE

Novel left-handed double-helical chiral carbon nanotube for electrochemical biosensing study

Received 00th January 20xx,
Accepted 00th January 20xx

DOI: 10.1039/x0xx00000x

www.rsc.org/

Shuang Ren,[a] Huan Wang,[a]* Yufan Zhang,[a] Liping Guo,[b] Hongyi Zhang,[a]* Zhihong Shi,[a] Yuena Sun,[a] Mingjie Li,[a] Meng Li,[a] Zheng Huang[a]

A novel left-handed double-helical chiral carbon nanotube (CCNT) was one-step synthesized by carbonization of self-assembled chiral polypyrrole nanotubes, which came from the electrostatic interaction between the carboxylic amphiphilic molecules and the pyrrole monomers. Different samples were prepared through changing the carbonization temperature. These samples were characterized by scanning electron microscopy (SEM), transmission electron microscopy (TEM), N_2 adsorption-desorption and X-ray Photoelectron Spectroscopy (XPS). We present the electrochemical biosensing performance of the prepared CCNT by using dopamine (DA), ascorbic acid (AA), uric acid (UA), H_2O_2 and NADH as probes. CCNT shows high electrocatalytic activity towards above molecules with a decrease of overpotential and a drastic enhancement of the anodic currents compared to the ordinary carbon nanotube. Moreover, the influence of carbonization temprature, pore size, different N-bonding configurations (pyridinic N, pyrrolic N and graphitic N) and surface area on electrocatalytic performance of the CCNT was studied in detail. Result shows that CCNT-900 with largest BET surface area and suitble N-bonding configurations exhibits the best electrocatalytic activity. The CCNT with remarkable electrochemical biosensing capability may be a kind of promising nanomaterial for electrochemical biosensing applications.

Introduction

In the past few years, the development of novel electrochemical catalyst with outstanding electrocatalytic performance has aroused extensive interests in electrochemistry filed. Among the numerous nanomaterials, carbon nanomaterial has attracted much attention, owing to their excellent physical and chemical properties[1, 2]. Some carbon nanomaterial such as carbon nanotubes[3], carbon nanofibers[4], graphene[5], ordered mesoporous carbon[6] and porous graphene[7] have been widely used in electrocatalytic field and showed outstanding electrocatalytic performance. Nevertheless, the research of novel carbon nanomaterial with new nanostructure, higher electrocatalytic activity and more unique electrochemical properties is still a major challenge.

Chirality phenomenon is widespread in nature, such as human hands, chiral amino acid, DNA macromolecule, chiral drugs and so on. Moreover, chiral molecules and materials can be designed to perform unique functions. Therefore, preparation of chiral nanomaterial has become a serious challenge to researchers. Chiral materials research is of great importance to bioscience, pharmacochemistry and material science. In recent years, chiral inorganic materials have attracted great interest, such as chiral mesoporous silica[8, 9], chiral metal nanoparticles[10, 11] and chiral nanocomposites[12]. Besides, chiral carbon is the most recently developed chiral nanomaterial which combines the advantages of carbon materials and chiral properties. It is a promising material in asymmetric catalysis[13], electrocatalysis and biosensor areas[14, 15]. However, up to now, the electrocatalytic application of chiral carbon nanomaterial has been rarely reported. In addition, most of the chiral carbon nanomaterials are mixtures of equal amounts of left- and right-handed structures, so the selective synthesis of enantiopure chiral carbon nanomaterial with high electrocatalytic activity is still a formidable challenge that remains unsolved.

Here, we prepared an enantiopure chiral carbon nanotube (CCNT) by carbonization of self-assembled chiral polypyrrole nanotube according to the previous reported work[16]. Three kinds of enantiopure left-handed CCNTs were synthesized at different carbonization temperatures (denoted as CCNT-500, CCNT-700 and CCNT-900, respectively). In our present work, CCNT was first employed as electrocatalyst in electrochemical area. Moreover, the influence of carbonization temperature, surface area and different N-bonding configurations on electrocatalytic performance was also researched. This work is of great significance for the successful application of enantiopure CCNT in electrocatalytic area.

[a] Key Laboratory of Analytical Science and Technology of Hebei Province, College of Chemistry and Environmental Science, Hebei University, Baoding 071002, Hebei Province, P. R. China. E-mail address: zwhsjzl@163.com; Fax: +86-0312-5079403; Tel.: +86-0312-5079403
[b] Faculty of Chemistry, Northeast Normal University, Changchun, 130024, P. R. China

Experimental

Reagents and apparatus

Dopamine (DA), ascorbic acid (AA), uric acid (UA), NADH and L-glutamic acid were purchased from Sigma-Aldrich (MO, USA). Acetone, myristoyl chloride, H_2O_2, pyrrole and ammonium persulfate were obtained from Aladdin Industrial Corporation (Shanghai, China). All other reagents were of analytical grade and used as received without further purification. Double-distilled water was used throughout the whole experiment. Phosphate buffer solution (PBS, 0.1M, pH 7.4) prepared from Na_2HPO_4, NaH_2PO_4 and H_3PO_4 was employed as a supporting electrolyte.

Electrochemical experiments were performed on a CHI 760E electrochemical workstation (Chenhua Instrument, China) with a conventional three-electrode system. The reference electrode is Ag/AgCl saturated with KCl and platinum wire as the counter electrode. The working electrode was a glassy carbon electrode (GCE) modified with enantiopure CCNT (CCNT/GCE). All experiments were performed at room temperature.

Scanning electron microscopy (SEM) images were determined with a JSM-7500FSEM (JEOL, Japan). Transmission electron microscopy (TEM) images were recorded on a Tecnai G2F20 S-TWIN transmission electron microscope (FEI, USA). Nitrogen adsorption-desorption isotherms were measured on an ASAP 2020 (Micromeritics, USA). The Brunauer-Emmett-Teller (BET) method was utilized to calculate the specific surface area. X-ray photoelectron spectra (XPS) were collected using an ESCALAB-MKII 250 photoelectron spectrometer (VG Co.) with Al-Ka X-ray radiation as the X-ray source for excitation.

Preparation of CCNT-x samples

Amino acid surfactant C_{18}-L-Glu was first prepared according to the following steps[17]: 35.5 g L-glutamic acid was dissolved in a mixture of deionized water (140 mL), acetone (120 mL) and NaOH (19.2 g). The obtained solution was stirred vigorously under 30 ℃, then 60.5 g myristoyl chloride was added into the mixture drop by drop in ice-cooling condition and 20 mL NaOH (0.2 M) was added to keep the pH (pH 12) simultaneously. The reaction mixture was stirred for additional 1 h and acidified to pH 1 with HCl. Finally, the surfactant C_{18}-L-Glu was obtained by washing the mixture with deionized water and petroleum ether to remove the unreacted myristoyl chloride and then freeze-drying under -60 ℃.

The enantiopure CCNT-x samples were obtained by a one-step carbonization of self-assembled chiral polypyrrole nanotubes according to the method reported by Liu et al [16]. In the typical procedure, C_{18}-L-Glu (0.06 mmol) was dissolved in methanol (12.9 mL), then pyrrole (2.4 mmol) and deionized water (60 mL) were added and stirred for 10 min. After that, 2.0 M precooled ammonium persulfate aqueous solution was added into the mixture and stirred for another 30 min. The chiral polypyrrole nanotube was obtained by filtering, washing and then drying above product at 40 ℃ in vacuum. Finally, the prepared chiral polypyrrole nanotube was carbonized at different temperatures (500, 700 and 900 ℃) for 6 h under an Ar atmosphere (rate: 1.5 ℃ min^{-1}). Then the enantiopure CCNT-x samples (CCNT-500, CCNT-700 and CCNT-900) were synthesized.

Preparation of the modified electrode

Typically, GCE was carefully polished before each experiment with 1, 0.3 and 0.05 μm alumina powder and then rinsed thoroughly with double distilled water between each polishing step. Then the cleaned electrode was dried with a high-purify nitrogen stream for the next modification. To prepare the modified electrode, 1 mg of the as-prepared CCNT-X sample was dispersed into 1 mL DMF to give a homogeneous suspension upon bath sonication. The CCNT-x/GCE was prepared by casting 5 μL of the suspension on the surface of the well-polished GCE and the solvent was allowed to dry under an infrared lamp.

Results and discussion

Characterization of CCNT-x

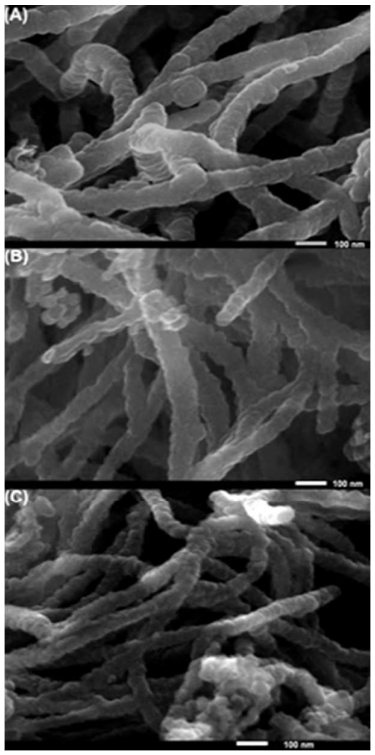

Fig. 1 SEM images of CCNT-500 (A), CCNT-700 (B) and CCNT-900 (C).

Fig. 1 and Fig. S1 show the SEM images of CCNT-500, CCNT-700 and CCNT-900. As can be clearly seen, the CCNTs are composed exclusively of left-handed double-helical nanotubes with uniform morphology. The diameters of the as-prepared CCNTs are in the range of 40-73 nm. Moreover, with the increase of carbonization temperature, the outer diameter of the nanotubes is slightly decreased and their surface become gradually folded, which can facilitate the electron transfer. However, the double-helical morphology of the nanotubes is still well-maintained at higher temperatures (900℃), thus

displaying the high ability to memorize the original morphology.

The TEM images in Fig. 2 indicate that the CCNTs possess helical inner tubes with a diameter of 13-19 nm. Moreover, CCNT carbonized at high temperature (900℃) shows a layered arrangement with a rough surface, which may be the characteristic structure of graphitized carbon [18]. This matches well with the following result of XPS. According to previous literature, polypyrrole can be carbonized to graphitized structures by dehydrogenation, during this process, polypyrrole chains grow and rearrangement[18].

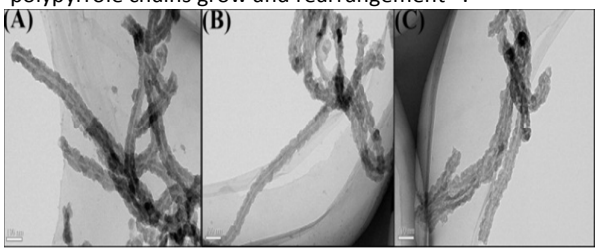

Fig. 2 TEM images of CCNT-500 (A), CCNT-700(B) and CCNT-900(C).

Fig. 3 presents N_2 adsorption-desorption isotherms and the corresponding pore size distribution curves of CCNTs. According to the IUPAC classification, three isotherms (Fig. 3A) exhibit typical Ⅳ type isotherm with a hysteresis loop that corresponds to capillary condensation taking place in mesopores. According to the Brunauer-Emmett-Teller (BET) method, we obtain that the surface area of CCNTs increase with the rise of carbonization temperature. The related data were listed in Table S1. Fig. 3B represents a pore size distribution focused on 20.8 nm for CCNT-500 and CCNT-700, while for CCNT-900, the pore size distribution centres at 9.7 and 22.8 nm, which may be attributed to the higher temperature during graphitization.

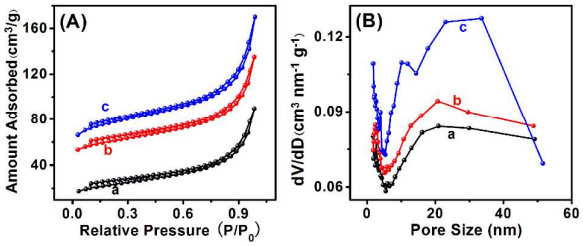

Fig. 3 (A) Nitrogen adsorption-desorption isotherms and (B) pore size distributions of CCNT-500 (a), CCNT-700 (b) and CCNT-900 (c).

The chemical compositions of CCNT-x samples were analysed by X-ray photoelectron spectroscopy (XPS, Fig. 4). As can be seen, the high resolution N1s XPS spectra can be deconvoluted into three different signals with binding energies of 398.0 (pyridinic N), 40 0.0 (pyrrolic N) and 401.3 eV (graphitic N) [19]. Moreover, the three peaks significantly change with the pyrolysis temperature, which indicates that different amount of N-bonding configurations are formed at different pyrolysis temperatures. Fig. 4D clearly shows the different amount of pyridinic N, pyrrolic N and graphitic N in CCNT-500, CCNT-700 and CCNT-900. At the pyrolysis temperature of 500 ℃, the amount of pyridinic N, pyrrolic N and graphitic N is 4.24%, 1.40% and 0.24%, respectively. When the pyrolysis temperature increased to 700 and 900 ℃, the amount of pyridinic N and pyrrolic N slightly decreased while graphitic N increased (Table S1). This is because pyridinic N and pyrrolic N are less stable at high temperatures, however, at high carbonization temperature, the degree of graphitization increase, so the amounts of graphitic N increase. The different amounts of N-bonding configurations in CCNT-x samples will have a significant influence on their electrocatalytic performances. The previous reports [19-21] have suggested that the content of nitrogen is crucial for the promotion of electrocatalytic activity.

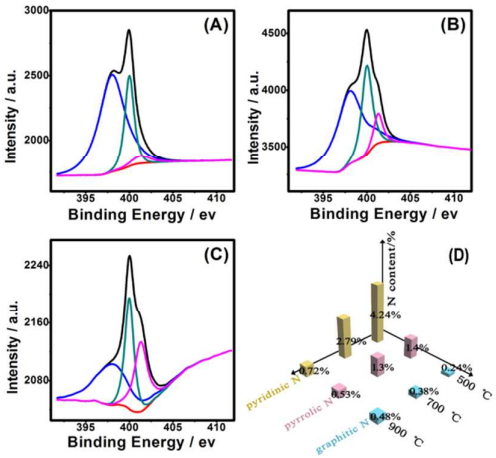

Fig. 4 High-resolution N1s XPS spectra of CCNT-500 (A), CCNT-700 (B) and CCNT-900(C), the signals fit into three energy components centered around 398.0 (pyridinic N), 400.0 (pyrrolic N) and 401.3 eV (graphitic N). (D) The content of three N-bonding configurations in CCNT-x samples.

Electrocatalytic oxidation of AA, DA and UA

In order to evaluate the electrocatalytic performance of the prepared CCNT-x samples, AA, DA and UA are employed as probes and multi-walled carbon nanotube (WCNT) is used for comparison. Fig. 5 A–C shows the cyclic voltammograms (CVs) of AA, DA and UA on GCE (curve a), WCNT/GCE (curve b), CCNT-500/GCE (curve c), CCNT-700/GCE (curve d) and CCNT-900/GCE (curve e) in 0.1 mol L^{-1} PBS. It can be noted from Fig. 5A, on the bare GCE, the oxidation peak of AA is broad and sluggish at a potential of 0.41 V, while on WCNT/GCE, AA oxidation occurs at a potential about 30 mV more negatively compared to the oxidation on GCE. Another important point to note is that the CCNT-x/GCE exhibits a sharp and strong oxidation peak with a sharply increase in the peak current compared with that of the WCNT/GCE. Moreover, CCNT-900/GCE shows the lowest peak potential (-0.014 V) and highest peak current among all the electrodes. Similarly, Fig. 5B and C display the oxidation of DA and UA on above electrodes, which exhibit the same results as the oxidation of AA. These results indicate that the CCNT-x/GCE exhibit accelerated electron transfer kinetics and can effectively catalyze the oxidation of AA, DA and UA. Furthermore, CCNT-900/GCE shows the best electrocatalytic activity among three CCNTs samples.

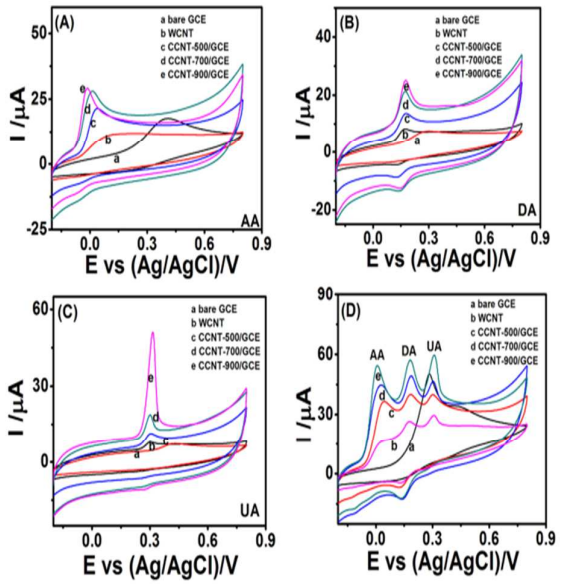

Fig. 5 CVs of bare GCE (a), WCNT/GCE (b), CCNT-500/GCE (c), CCNT-700/GCE (d) and CCNT-900/GCE (e) in the presence of 1 mM AA (A), 200 μM DA (B), 150 μM UA (C) and 2 mM AA, 500 μM DA and 500 μM UA (D) in 0.1 M PBS (pH 7.4), scan rate: 50 mV s^{-1}.

In addition, the electrochemical responses of the ternary mixture containing 2 mM AA, 0.5 mM DA and 0.5 mM UA on different electrodes were also investigated. As shown in Fig. 5D, it is clear that the peak potentials of AA, DA and UA are found to be overlapped on the GCE, which demonstrates that GCE cannot successfully separate and detect these biomolecules. While on WCNT/GCE, three weak peaks are obtained with low peak current. However, when the electrode is modified by CCNT-x, AA, DA and UA exhibit three completely separated anodic peaks with sharply increased current. Moreover, the oxidation of the three species occurs at more negative potential on CCNT-x/GCE compared with that on WCNT/GCE. Furthermore, the response currents of the three species on CCNT-900/GCE are much higher than on the other two electrodes. The peak potential separation for AA-DA and DA-UA are 174 mV and 125 mV, respectively. The result suggests that CCNT-900/GCE offers a special advantage for the simultaneous electrochemical detection of AA, DA and UA.

Electrochemical detection of AA, DA and UA

Additionally, DPV responses of the CCNT-900/GCE towards simultaneous detection of DA, AA and UA were investigated when the concentration of one species changed with the other two keeping constant. Fig. 6A shows the DPVs recorded on CCNT-900/GCE in solutions containing various concentrations of AA in the presence of 5 μM DA and 10 μM UA. It can be clearly seen that the peak current response for the oxidation of AA rises linearly with the increasing concentration of AA, while the current responses of DA and UA keep nearly unchanged, indicating that the coexistence of DA and UA do not interfere with the electro oxidation of AA. The linear range of AA is 10 μM - 1.28 mM with a detection limit of 1.33 μM. The RSD is 1.7% at LOQ level. Similarly, as shown in Fig. 6B and C, when keeping the concentrations of other two compounds constant, the oxidation peak current of DA or UA also increases linearly with their respective concentration, while the current responses of the other two coexisted species keep unchanged. All the data of Fig. 6 are listed in Table S2.

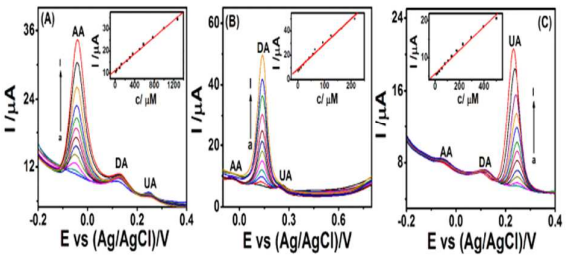

Fig. 6 (A) DPVs of different concentration AA in the presence of 5 μM DA and 10 μM UA on CCNT-900/GCE. AA concentrations (a to l): 10, 30, 90, 130, 240, 300, 360, 500, 580, 770, 1000 and 1280 μM. (B) DPVs of different concentration DA in the presence of 80 μM AA and 20 μM UA on CCNT-900/GCE. DA concentrations (a to l): 1, 6, 12, 20, 30, 42, 56, 64, 94, 124, 164 and 214 μM. (C) DPVs of different concentration UA in the presence of 50 μM AA and 3 μM DA on CCNT-900/GCE. UA concentrations (a to l): 10, 20, 35, 55, 80, 105, 135, 175, 225, 295, 395 and 500 μM. Insets are linear relationships between peak currents and concentrations. Electrolyte: 0.1 M PBS (pH 7.4). Pulse amplitude: 0.05 V. Pulse width: 0.05 s. Pulse period: 0.5 s.

In addition, DPVs of simultaneous detection of AA, DA and UA on CCNT-900/GCE are depicted in Fig. 7. As can be clearly observed, the three anodic peaks are well separated from each other with a potential difference of 120 and 160 mV for AA-DA and DA-UA, respectively. Moreover, from the calibration curve, we obtained that the peak current of the three species rises linearly with their respective concentration. The linear ranges are 5.0-1080 μM, 0.1-111.6 μM and 0.5-540 μM for AA, DA and UA, respectively. The corresponding linear regression equations are listed as follow: I (μA) = 10.84+0.0095 c_{AA} (μM) (R^2=0.9903), I (μA) = 8.29+0.226 c_{DA} (μM) (R^2=0.9936), I (μA) = 7.74+0.0308c_{UA} (μM) (R^2=0.9915).

All the results above strongly suggest that CCNT-900/GCE can realize simultaneous detection of AA, DA and UA in their ternary mixture with wide liner range, low detection limit and high sensitivity, indicating the excellent electrocatalytic activity of the prepared CCNT-900.

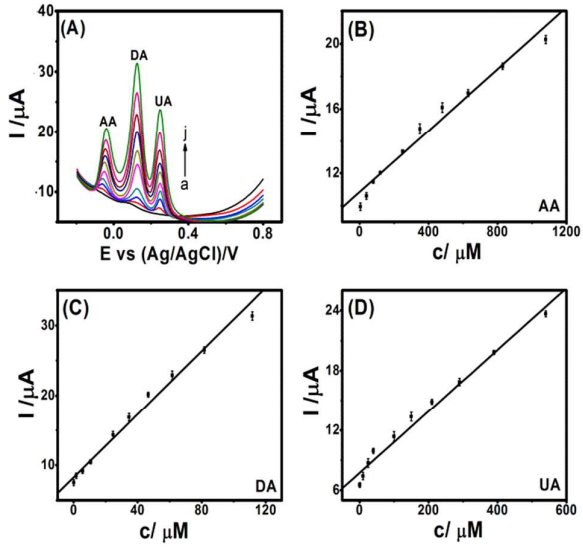

Fig. 7 (A) DPVs of different concentrations of AA, DA and UA on CCNT-900/GCE in 0.1 M PBS. AA concentrations (μM, a-j) 5.0, 40, 80, 120, 250, 350, 480, 630, 830 and 1080 μM; DA concentrations (μM, a-j) 0.1, 1.6, 5.6, 10.6, 16.6, 24.6, 34.6, 46.6, 61.6, 81.6 and 111.6 μM; UA concentrations (μM, a-j) 0.5, 10, 25, 40, 100, 150, 210, 290, 390 and 540 μM. Pulse amplitude: 0.05 V. Pulse width: 0.05 s. Pulse period: 0.5 s. (B-D) The linear relationship between concentration and current signal for AA, DA and UA, respectively.

Amperometric detection of AA, DA and UA

Moreover, we have successfully performed the determination of AA, DA and UA through the amperometric method Fig. S2 shows the amperometric response of CCNT-900/GCE with successive addition of different concentrations of AA, DA or UA. Insets clearly show the amperometric response of each compound at low concentration on CCNT-900/GCE. As observed in the current staircases, the response current changes rapidly even at very low concentrations of AA, DA or UA. Besides, CCNT-900/GCE exhibits a wide linear response between the current and concentration in the range of 0.5-1500 μM, 0.1-200 μM and 0.02-200 μM for AA, DA and UA, respectively (Fig. S2 B, D, F). The linear regression equations are as follows: I (μA) = 1.9+0.01785 c_{AA} (μM) (R^2=0.9924); I (μA) = 2.88+0.216 c_{DA} (μM) (R^2=0.9899); I (μA)=2.29+0.0.0851 c_{UA} (μM) (R^2=0.9994). The detection limits are calculated to be 0.175, 0.014 and 0.0165 μM with the signal to noise ratio of three (S/N=3) for AA, DA and UA, respectively. All the above results indicate the excellent electrocatalytic performance of CCNT-900/GCE.

Reproducibility and stability

To investigate the reproducibility of CCNT-900/GCE, repetitive measurements have been carried out for simultaneous detection of 100 μM AA, 10 μM DA and 40 μM UA in their mixture. The RSD of current signal are 1.9%, 3.98% and 0.5% for five measurements for AA, DA and UA on the same electrode, respectively. This indicates that the modified electrode does not undergo surface fouling during the measurements. The modified electrode also shows high stability. When the CCNT-900/GCE was stored in PBS (pH 7.4) at room temperature for a week, the current response remained 94.6%, 95.7% and 96.8% of its original value for AA, DA and UA, respectively, suggesting the long-term stability of the modified electrode.

Electrochemical detection of H_2O_2

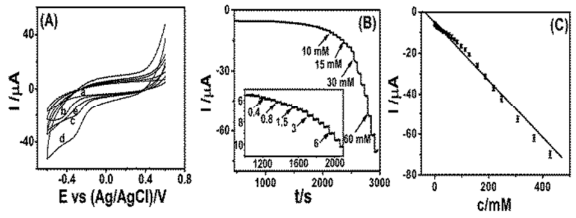

Fig. 8 (A) CVs of GCE (a), WCNT/GCE (b), CCNT-500/GCE (c), CCNT-700/GCE (d) and CCNT-900/GCE (e) in the presence of 2.0 mM H_2O_2. Scan rate: 50 mV s^{-1}. (B) Typical amperometric current-time curve of CCNT-900/GCE with successive additions of different concentration H_2O_2 (mM). Inset: The amperometric response with successive addition of H_2O_2 at lower concentration. (C) The linear relationship between H_2O_2 concentration and current signal on CCNT-900/GCE. Electrolyte: 0.1 M PBS (pH 7.4).

To further investigate the electrocatalytic activity of the CCNT-x samples, electrochemical detection of H_2O_2 was researched. Fig. 8A shows the CVs of H_2O_2 reduction on different electrodes in 0.1 M PBS (pH=7.4). As can be clearly seen, the CCNT-x/GCE exhibits superior electrochemical response to H_2O_2 compared to bare GCE and WCNT/GCE. Moreover, the CCNT-900/GCE performs the best electrocatalytic activity among the synthesized electrode materials towards H_2O_2 reduction. Obviously, the presence of CCNT-900/GCE makes the electron transfer much easier compared with that of other CCNT-x samples. On the basis of the electrochemical response of CCNT-900/GCE towards H_2O_2, quantitative detection of H_2O_2 was further carried out using amperometric current-time method. Fig. 8B presents the amperometric responses of CCNT-900/GCE for each successive addition of different amount of H_2O_2 in 0.1 M PBS (pH 7.4). Inset curve shows the current response of H_2O_2 at low concentration on CCNT-900/GCE. As directly perceived through current staircases, the response of CCNT-900/GCE dramatically increased after each addition of H_2O_2 into PBS and rapidly reached to a platform. Moreover, response current shows a linear relationship (Fig. 8C) with H_2O_2 concentration over the tested range of 20 μM-60 mM. The detection limit is estimated to be 2 μM with the signal to noise ratio of three (S/N=3). The RSD is 2.7% at LOQ level. The electrocatalytic performance of CCNT-900/GCE was compared with other H_2O_2 sensors in Table S3.

Electrochemical detection of NADH

The electrocatalytic properties of different electrodes toward NADH detection were also investigated. Fig. 9A displays the CVs of bare GCE, WCNT/GCE and CCNT-x/GCE in the presence of 1 mM NADH. As can be obviously seen, there is negligible

current response on bare GCE, while on WCNT/GCE, a slightly enhanced current response can be observed. However, on CCNT-x/GCE, the electrochemical response significantly enhanced. Additionally, the CCNT-900/GCE performs the best electrocatalytic activity towards NADH oxidation compared with that of other CCNT-x samples, which indicates that the presence of CCNT-900 accelerates electron transfer. Fig. 9B displays the current-time curve with successive addition of different concentrations of NADH. The applied potential was chosen at +0.4 V based on the CV measurement. Inset curve shows the current response of NADH at low concentration on CCNT-900/GCE. As it shows in Fig.9C, the current increased linearly with the linear ranges from 0.1 to 400 μM for NADH detection. The linear regression equation is I (μA) = 2.65+0.0835 c_{NADH} (μM) (R^2=0.9960) with a detection limit of 0.035 μM (S/N=3). The RSD is 1.5% at LOQ level. The electrocatalytic property of CCNT-900/GCE was compared with other NADH sensors in Table S4, indicating high performance of CCNT-900/GCE.

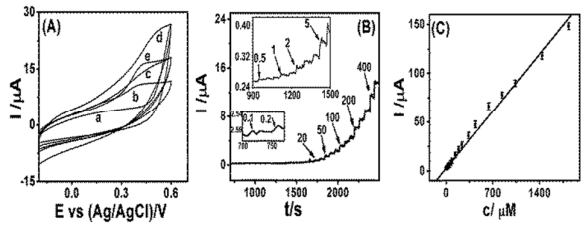

Fig. 9 (A) CVs of GCE (a), WCNT/GCE (b), CCNT-500/GCE (c), CCNT-700/GCE (d) and CCNT-900/GCE (e) in the presence of 1 mM NADH. Scan rate: 50 mV s^{-1}. (B) Typical amperometric current-time curve of CCNT-900/GCE with successive additions of different concentration NADH (μM). Inset: The amperometric response with successive addition of NADH at lower concentration. (C) The linear relationship between NADH concentration and current signal on CCNT-900/GCE.

According to all the characterization results mentioned above, with the increase of the carbonization temperature, amount of graphitic N, pore size and surface area increase accordingly (Table S1). In addition, it can be clearly observed from the results that the CCNT-900/GCE performs the best electrocatalytic activity towards above molecules among the synthesized samples in this study, which demonstrates that the carbonization temperature, pore size distribution, surface area and N-bonding configurations have a significant influence on the electrocatalytic performances of carbon nanomaterial. Moreover, high carbonization temperature and amount of graphitic N, large surface area and pore size lead to high electrocatalytic activity. This can be attributed to the large surface area and suitable N-bonding configurations in CCNT-900 which can provide more active sites and accelerate the electron transfer between the electrode and species in solution. Moreover, the large pore size can accelerate the mass transport of reactant molecule. Therefore, the novel carbon materials with unique structure characteristic may have significant applications in electrochemical biosensing research area.

Conclusions

In this work, three kinds of left-handed double-helical chiral carbonaceous nanotubes (CCNTs) have been successfully prepared by one step carbonization of self-assembled chiral polypyrrole nanotube at different temperatures. Characterization data indicates that carbonization temperatures have great influence on the BET surface areas and the amount of different N-bonding configurations, which are closely related to the electrocatalytic performance of CCNT-x. The experimental results show that the proposed CCNT-900 shows the highest electrocatalytic activity towards the oxidation of AA, DA, UA, NADH and the reduction of H_2O_2 at low overpotential, with many desired properties including low detection limit, satisfactory linear concentration range and excellent stability. The superior eletrocatalytic performance indicates that it is a very promising catalyst candidate for electrochemical biosensors.

Acknowledgements

The authors gratefully acknowledge the support of the National Natural Science Foundation of China (No. 21505031), science technology research and development guidance programme project of Baoding City (No. 14ZG031) and colleges and universities science technology research project of Hebei Province (No. Z2015096).

Notes and references

1 K.X. Li, Y.H. Luo, Z.X. Yu, M.H. Deng, D.M. Li and Q.B. Meng, Low temperature fabrication of efficient porous carbon counter electrode for dye-sensitized solar cells. *Electrochem Commun*, 2009, **11**, 1346.
2 T.T. Baby, S.S.J. Aravind, T. Arockiadoss, R.B. Rakhi and S. Ramaprabhu, Metal decorated graphene nanosheets as immobilization matrix for amperometric glucose biosensor. *Sens Actuators B*, 2010, **145**, 71.
3 A. Kutluay and M. Aslanoglu, An electrochemical sensor prepared by sonochemical one-pot synthesis of multi-walled carbon nanotube-supported cobalt nanoparticles for the simultaneous determination of paracetamol and dopamine. *Anal Chim Acta*, 2014, **839**, 59.
4 L.L. Li, T.T. Zhou, G.Y. Sun, Z.H. Li, W.X. Yang, J.B. Jia and G.C. Yang, Ultrasensitive electrospun nickel-doped carbon nanofibers electrode for sensing paracetamol and glucose. *Electrochim Acta*, 2015, **152**, 31.
5 C. Wu, Q. Cheng, K.B. Wu, G. Wu and Q. Li, Graphene prepared by one-pot solvent exfoliation as a highly sensitive platform for electrochemical sensing. *Anal Chim Acta*, 2014, **825**, 26.
6 C.W. Zhang, L.B. Xu, N.N. Shan, T.T. Sun, J.F. Chen and Y.S. Yan, Enhanced electrocatalytic activity and durability of Pt particles supported on ordered mesoporous carbon spheres. *ACS Catalysis*, 2014, **4**, 1926.
7 H. Wang, X.J. Bo and L.P. Guo, Electrochemical biosensing platform based on a novel porous graphene nanosheet. *Sens Actuators B*, 2014, **192**, 181.
8 S.N. Che, Z. Liu, T. Ohsuna, K. Sakamoto, O. Terasaki and T. Tatsumi, Synthesis and characterization of chiral mesoporous silica. *Nature*, 2004, **429**, 281.

9 B. Wang, C. Chi, W. Shan, Y.H. Zhang, N. Ren, W.L. Yang and Y. Tang, Chiral mesostructured silica nanofibers of MCM-41. *Angewandte Chemie*, 2006, **118**, 2142.
10 T.G. Schaaff and R.L. Whetten, Giant gold-glutathione cluster compounds: intense optical activity in metal-based transitions. *J Phys Chem B*, 2000, **104**, 2630.
11 C. Gautier and T. Bürgi, Chiral gold nanoparticles. *ChemPhysChem*, 2009, **10**, 483.
12 J.J Xie, Y.Y Duan and S.N. Che, Chirality of metal nanoparticles in chiral mesoporous silica. *Adv Funct Mater*, 2012, **22**, 3784.
13 L. Xing, J.H. Xie, Y.S. Chen, L.X. Wang and Q.L. Zhou, Simply modified chiral diphosphine: catalyst recycling via non-covalent absorption on carbon nanotubes. *Adv Synth Catal*, 2008, **350**, 1013.
14 R.J. Cui, X.Y. Wang, G.H. Zhang and C. Wang, Simultaneous determination of dopamine, ascorbic acid, and uric acid using helical carbon nanotubes modified electrode. *Sens Actuators B*, 2012, **161**, 1139.
15 D.K. Huang, B.Y. Zhang, J. Bai, Y.B. Zhang, G. Wittstock, M.K. Wang and Y. Shen, Pt catalyst supported within TiO_2 mesoporous films for oxygen reduction reaction. *Electrochim Acta*, 2014, **130**, 97.
16 S.H. Liu, Y.Y. Duan, X.J. Feng, J. Yang and S.N. Che, Synthesis of enantiopure carbonaceous nanotubes with optical activity. *Angew Chem Int Edit*, 2013, **52**, 6858.
17 Y.T. Yu, H.B. Qiu, X.W. Wu, H.C. Li, Y.S. Li, Y. Sakamoto, Y. Inoue, K. Sakamoto, O. Terasaki and S.N. Che, Synthesis and characterization of silica nanotubes with radially oriented mesopores. *Adv Funct Mater*, 2008, **18**, 541.
18 Y.W. Ma, S.J. Jiang, G.Q. Jian, H.S. Tao, L.S. Yu, X.B. Wang, X.Z. Wang, J.M. Zhu, Z. Hu and Y. Chen, CNx nanofibers converted from polypyrrole nanowires as platinum support for methanol oxidation. *Energy Environ Sci*, 2009, **2**, 224.
19 S.B. Yang, X.L. Feng, X.C. Wang and K. Müllen, Graphene-based carbon nitride nanosheets as efficient metal-free electrocatalysts for oxygen reduction reactions. *Angew Chem Int Ed*, 2011, **50**, 5339.
20 R.L. Liu, D.Q. Wu and X.L. Feng, Nitrogen-doped ordered mesoporous graphitic arrays with high electrocatalytic activity for oxygen reduction. *Angew Chem*, 2010, **122**, 2619.
21 L.T. Qu,Y. Liu, J-B. Baek and L.M. Dai, Nitrogen-doped graphene as efficient metal-free electrocatalyst for oxygen reduction in fuel cells. *ACS Nano*, 2010, **4**, 1321.

Graphical Abstract

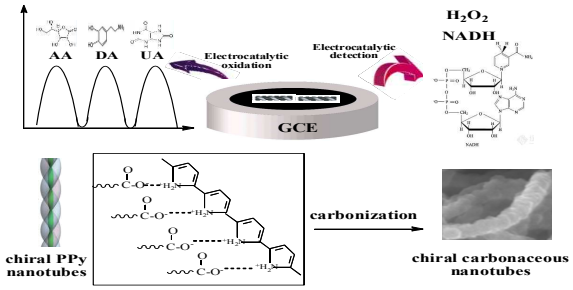

The preparation and electrochemical biosensing application of novel left-handed double-helical chiral carbon nanotube.